Importance of salinity barrier layer for the buildup of El Niño

C. Maes, J. Picaut, S. Belamari

Importance of the Salinity Barrier Layer for the Buildup of El Niño

CHRISTOPHE MAES AND JOËL PICAUT

Laboratoire d'Etudes en Géophysique et Océanographie Spatiales, Institut de Recherche pour le Développement, Toulouse, France

SOPHIE BELAMARI

Centre National de Recherches Météorolgiques, Météo-France, Toulouse, France

(Manuscript received 14 August 2003, in final form 20 April 2004)

ABSTRACT

Several studies using sea level observations and coupled models have shown that heat buildup in the western equatorial Pacific is a necessary condition for a major El Niño to develop. However, none of these studies has considered the potential influence of the vertical salinity stratification on the heat buildup and thus on El Niño. In the warm pool, this stratification results in the presence of a barrier layer that controls the base of the ocean mixed layer. Analyses of in situ and TOPEX/Poseidon data, associated with indirect estimates of the vertical salinity stratification, reveal the concomitant presence of heat buildup and a significant barrier layer in the western equatorial Pacific. This relationship occurs during periods of about one year prior to the mature phase of El Niño events over the period 1993–2002. Analyses from a coupled ocean–atmosphere general circulation model suggest that this relationship is statistically robust. The ability of the coupled model to reproduce a realistic El Niño together with heat buildup, westerly wind bursts, and a salinity barrier layer suggests further investigations of the nature of this relationship. In order to remove the barrier layer, modifications to the vertical ocean mixing scheme are applied in the equatorial warm pool and during the 1-yr period of the heat buildup. At the bottom of the ocean mixed layer, the heat buildup is locally attenuated, as expected from switching on the entrainment cooling. At the surface, the coupled response over the warm pool increases the fetch of westerly winds and favors the displacement of the atmospheric deep convection toward the central equatorial Pacific. These westerly winds generate a series of downwelling equatorial Kelvin waves whose associated eastward currents drain the heat buildup toward the eastern Pacific Ocean. The overall reduction of the heat buildup before the onset of El Niño results in the failure of El Niño. These coupled model analyses confirm that the buildup is a necessary condition for El Niño development and show that the barrier layer in the western equatorial Pacific is important for maintaining the heat buildup.

1. Introduction

On interannual time scales, the climate of the tropical Pacific Ocean is dominated by the El Niño–Southern Oscillation (ENSO) phenomenon. This phenomenon results from the interaction between the surface winds and the sea surface temperature (SST), as highlighted by Bjerknes (1969). The oscillatory nature of ENSO is linked to the subsurface adjustment of the ocean that provides the memory of the coupled ocean–atmosphere system. Wyrtki (1975, 1985) and Cane and Zebiak (1985), using respectively, sea level observations and a simple coupled ocean–atmosphere model, found that the period between two El Niño events corresponds to the time required to recharge the equatorial band with warm water. In Wyrtki's (1975) view, the buildup of heat in the western Pacific is a precursor of El Niño. This mechanism contrasts with the delayed oscillator theory (Schopf and Suarez 1988; Battisti and Hirst 1989), which became the leading paradigm for ENSO during the Tropical Ocean Global Atmosphere (TOGA) program. In this theory, the adjustment period is controlled by the time required for equatorial Rossby waves to propagate westward, reflect at the western boundary, and propagate eastward as equatorial Kelvin waves. Jin (1997a,b) developed a conceptual recharge model that embodies the delayed oscillator, but ignores the explicit role of wave propagation. This model combines the dynamics of the SST–wind interaction with the nonequilibrium response between the mean thermocline depth and the surface wind stress. Using a compilation of different in situ datasets including subsurface temperature, Meinen and McPhaden (2000) demonstrate that the concept developed by Jin (1997a,b) is in agreement with observations over the period 1980–99. While variations in SST, zonal wind stress, and the east–west slope of the thermocline are all nearly in phase within the equatorial band, the heat buildup leads each of these

Corresponding author address: Dr. Christophe Maes, LEGOS, IRD, 18 Evenue Belin, 31401 Toulouse Cedex 4, France.
E-mail: Christophe.Maes@cnes.fr

variables by an average of 7 months. These studies suggest that the equatorial heat buildup is an intrinsic element of El Niño.

The detailed mechanisms involved in the heat buildup in the western equatorial Pacific have received, paradoxically, little consideration since the pioneering work of Wyrtki (1975, 1985). The presence of meridional boundaries in the oceans, in addition to the stress of the trade winds, is regarded as the major reason for the accumulation of warm water. Zebiak (1989) argues that variations in heat buildup are dynamically rather than thermodynamically induced. He also shows that equatorial dynamics are more effective in controlling the evolution of heat content than the dynamics at higher latitudes and the dynamics of the western boundary region. The variability in the heat buildup prior to the development of El Niño has been used to explore the predictability of the tropical Pacific climate (e.g., Latif and Flügel 1991). By analyzing forecasts from a simple coupled model, Perigaud and Cassou (2000) found that the impact of westerly wind bursts (WWBs) on ENSO predictions also depends on the ocean heat buildup, especially during recent strong El Niño events. The relative importance of these different mechanisms in the development of an El Niño is still subject to debate. For example, it is not guaranteed that the buildup amplitude must reach a given threshold before an El Niño and even if this condition is necessary and/or sufficient. A detailed analysis of physical mechanisms involved in the buildup and a demonstration of their pertinence for El Niño prediction are yet to be established.

An increase in the strength of easterly winds in the central Pacific generates upwelling equatorial Rossby waves characterized by westward currents and by westward propagation. These waves are associated with a positive pressure perturbation that raises the sea level in the western Pacific. Li and Clarke (1994) confirm that a 3-month lag between the trade winds in the central Pacific and the sea level in the western Pacific is associated with the time required for Rossby waves to propagate into the region. They also noted that significant correlations between these phenomena could occur with lags as long as one year. Their result is consistent with the time evolution of positive sea level anomalies that has been described as a precursor mode for the onset of an El Niño event. This mode has been derived from different datasets and several statistical methods (e.g., Latif and Flügel 1991; Xue et al. 2000; Meinen and McPhaden 2000). A question that comes to mind is why local wind forcing or other local processes do not dissipate the buildup. In the western Pacific, observations have revealed that the mixed layer is insulated from deep and cold waters by strong salinity stratification within the warm isothermal surface waters (Lindstrom et al. 1987; Lukas and Lindstrom 1991; Sprintall and Tomczak 1992; Ando and McPhaden 1997). The difference in depth between the bottom of the isothermal layer and the bottom of the mixed layer is the barrier layer thickness (BLT). The barrier layer serves to inhibit the entrainment of cold water from below into the mixed layer. The effects of the barrier layer on the dynamics of the warm pool have been shown to be important during the onset of El Niño in a coupled model where the removal of the barrier layer was able to reduce or abort El Niño (Maes et al. 2002b). However, the role of the barrier layer during El Niño has not been fully investigated.

The main purpose of this study is to explore whether the salinity barrier layer is important in maintaining the heat buildup in the western Pacific prior to El Niño. The relationship between the barrier layer and the buildup could be important, as suggested in Fig. 1, which displays longitude–time plots, averaged between 2°N and 2°S, of SST and thermosteric anomalies together with an estimate of the BLT. Because of sparse observations of salinity profiles, the salinity variability is determined by an indirect approach that combines the temperature data of the Tropical Atmosphere Ocean/Triangle Trans-Ocean Buoy Network (TAO/TRITON) array, TOPEX/Poseidon sea level anomalies, and a set of vertical empirical orthogonal functions derived from conductivity–temperature–depth profiles (Maes and Behringer 2000). The thermosteric anomalies are computed by replacing the variable salinity profiles by their mean profile in the computation of dynamic height anomaly referenced to 500 dbar. These thermosteric anomalies are better suited than the standard dynamical height anomalies to study the heat buildup in the western Pacific because the halosteric contribution to dynamic height is not negligible and is of opposite sign to the thermosteric contribution (Maes et al. 2002a). The BLT is computed as the difference between the depth where the temperature differs from SST by 0.5°C and the depth of the mixed layer where the density differs from the surface density by 0.125 kg m^{-3}. As shown in Fig. 1, the El Niño events over the period 1993–2002 are characterized by a warming in the east together with an eastward displacement of the warm pool as defined by the 28.5°C isotherm. Prior to these events, a buildup of warm water is evident and simultaneous with the presence of a large BLT in the western Pacific. A detailed analysis of this particular relationship requires basinwide information on both surface and subsurface ocean states that is currently impossible to assemble from observations. The outputs of general circulation models (GCMs) provide a useful alternative if such models are able to reproduce similar features to those shown in Fig. 1.

The rest of the paper is organized as follows. Section 2 starts with a description of the coupled model with an emphasis on the simulated mean state and the seasonal cycle for the control experiment. Section 3 examines the relationship between the model heat buildup and the BLT in relation to El Niño. The analyses are focused on a strong El Niño simulated by the model that will highlight the combined role of the heat buildup and the BLT prior to this event. The importance of the relationship between the heat buildup and the BLT is

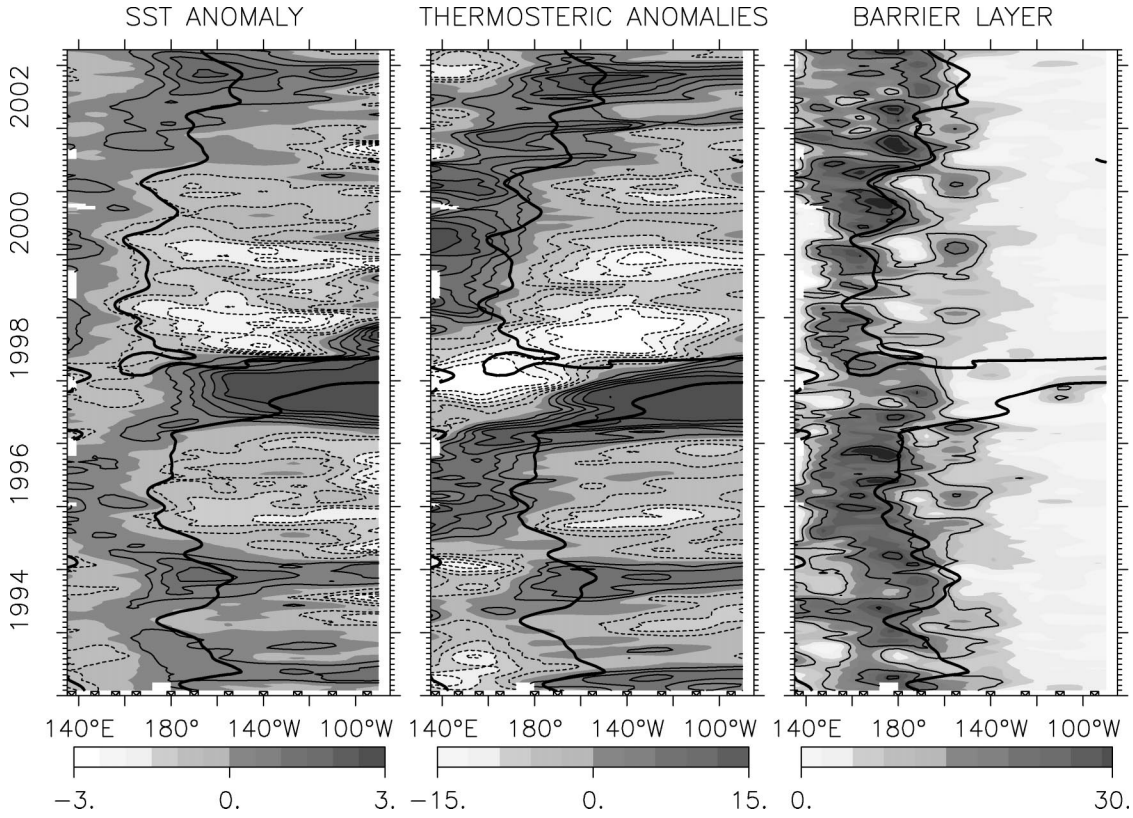

FIG. 1. Time–longitude sections averaged between 2°N and 2°S of interannual SST anomalies, thermosteric anomalies referenced to 500 m, and barrier layer thickness. The temperature field is provided by the TAO/TRITON observations, whereas the salinity field is derived from an indirect approach (see the text for explanation). The thin black line represents the 28.5°C SST isotherm. The contour interval is set to 0.5°C, 3 dyn cm, and 10 m. Dashed contours correspond to negative values.

tested in two-stage perturbed experiments. In the first stage, the dependency of the ocean vertical mixing scheme on the salinity stratification is removed within the equatorial warm pool during a 1-yr period. This year corresponds approximately to the heat buildup period prior to the El Niño event. In the second stage, the salinity dependency in the vertical mixing scheme is restored and the experiment continues. The idea is to perturb the model only during the buildup year so that subsequent analyses of model variability can be tied unambiguously back to that period. Because the tropical atmosphere exhibits significant internal variability that could disrupt El Niño, six-member ensembles of both the perturbed and control experiments have been generated to test the robustness of the effects of heat buildup and the BLT on El Niño. The physical processes involved during the buildup period prior to El Niño are analyzed in section 4. Comparable experiments are run for two other El Niño events and their similarities with the main experiment are examined before presenting conclusions in the last section.

2. The coupled model and simulated variability

The coupled model used in this study consists of the Météo-France atmospheric general circulation model (AGCM) and of the oceanic GCM (OGCM) developed at the Laboratoire d'Océanographie Dynamique et de Climatologie (LODYC). The AGCM was adapted for climate studies from the ARPEGE forecast model and is described by Déqué et al. (1994). In this study, a spectral T31 triangular horizontal truncation is used that corresponds to a resolution of 3.75° in the Tropics. The vertical discretization uses a hybrid sigma-pressure coordinate with 19 levels extending up to 10 hPa. The physical parameterizations include the radiation scheme developed by Morcrette (1990); deep and shallow convection are based on the mass-flux scheme of Bougeault (1985) and on a simple modification of the Richardson number (Geleyn 1987). The different coefficients employed in the convection and cloudiness treatment are derived from the sensibility analyses detailed in Terray (1998).

The OGCM is based on the Océan Parallélisé (OPA) code (Madec et al. 1998), and the present version is a tropical Pacific basin version adapted by Maes et al. (1997). The domain covers the tropical Pacific between 120°E and 70°W with 1° zonal resolution and is closed at 30°N and 30°S. The latitudinal resolution varies gradually from 0.5° at the equator to 2° at the northern and southern boundaries. Poleward of the 15°N–15°S band

and below the mixed layer, a linear restoring term damps the solution toward the seasonal-varying climatology of Levitus (1982). The model has 25 layers in the vertical with 10-m resolution in the upper 150 m. The maximum ocean depth is limited to 4500 m, but both bottom topography and coastlines are realistic. The solar radiation is allowed to penetrate the upper layers. The parameterization of vertical diffusion is based on a 1.5 turbulent kinetic energy closure scheme (Blanke and Delecluse 1993). The lateral diffusion uses a classical second-order operator whose coefficient corresponds to a medium value as discussed in Maes et al. (1997).

The coupling between the ocean and atmosphere models is achieved through the exchange, on a daily mean basis, of the fields of SST, surface wind stress, solar and net heat fluxes, and precipitation minus evaporation. The seasonal-varying climatology from Reynolds and Smith (1995) over the period 1979–88 is used to prescribe SST outside the OGCM domain. A smoothing procedure is applied to the SST near the poleward boundaries of the ocean model in order to adjust the net heat flux component exchanged between models. No flux correction is applied within the 15°S–15°N band and the coupling between the ocean and the atmosphere is completely free within this region. The initial conditions are obtained from independent forced integrations of each model and, because of the initial shock when the components are coupled, only the outputs from year 8 to year 40 are analyzed in the rest of this paper. During this period, the surface fields exchanged between the models do not exhibit significant long-term tendencies. The climate drift of the coupled model is relatively low with a negative tendency in the upper 300-m ocean temperature of less than 0.3°C over the 40 years (Belamari 2002).

Although ENSO modeling has made significant progress during the last decade, several intercomparisons of coupled GCMs have revealed that errors in SST could be large and systematic in the equatorial Pacific and that ENSO variability reproduced by models is often weak and/or incorrectly simulated. A complete description of the variability simulated by the present model is beyond the scope of this study, but it is important to verify that the mean state, the seasonal cycle, and the interannual variability of the key variables are consistent with the observations. The annual-mean simulated SST along the equator exhibits an east–west gradient with SSTs greater than 28°C in the western Pacific and SSTs around 26°C in the eastern Pacific. In this latter region, the model SST is characterized by a warm bias of about 1°C compared to observed climatologies, which is reasonable for models with coarse resolution (e.g., Mechoso et al. 1995). The annual-mean simulated zonal wind stress along the equator shows a more complex structure in its biases with stronger than observed wind stress in both the far western and the eastern Pacific and lower than observed wind stress in the central Pacific. These biases result in the underestimation of the southeastern trade winds in the Southern Hemisphere and in an overly strong penetration of the northeastern trade winds in the Northern Hemisphere (see Fig. 2 in Belamari et al. 2003).

The seasonal cycles of SST and zonal wind stress represent other key elements, as they serve to define the interannual anomaly. The left and center panels of Fig. 2 display the mean seasonal cycles of SST and zonal wind stress along the equatorial band. The main features of the SST observed seasonal cycle are well captured by the coupled model, with an annual harmonic that peaks in magnitude at around 100°W and displays a maximum development of the cold tongue in August–September. It must be noted, however, that the cold tongue does not persist long enough into the boreal winter and that the aforementioned mean warm bias in the eastern Pacific occurs during the warm season in April–May when the trade winds relax. In late summer, the strong development of the cold tongue induces a westward displacement of the warm pool that is too pronounced in the model. In the western Pacific, the waters warmer than 29°C are not always present throughout the year but this cold bias is less than 0.5°C, as shown by the permanent presence of waters warmer than 28.5°C westward of the date line (see the dark line in Fig. 2). The presence of these warm waters is necessary to trigger deep convection in the atmosphere as shown by the relationship between the SST and the outgoing longwave radiation (e.g., Webster et al. 1998). Despite the aforementioned differences, it is clear that the model captures the main features of the SST seasonal cycle quite realistically.

Similar conclusions hold for the zonal wind stress evolution, which shows the east-to-west phase propagation with a clear dominance of a semiannual cycle in the east between 180° and 120°W and an annual cycle west of the date line (Fig. 2b). The position of the southeasterly winds in late boreal winter is, however, located too far to the east and the strength of the easterly winds in summer is too strong as compared to the analyses of Yu and McPhaden (1999). In the western Pacific, the presence of westerly winds in winter is related to strong intraseasonal activity. It is important to note that this coupled model is able to naturally generate WWBs, whose the role in triggering a warm event was studied by Belamari et al. (2003).

The right-hand side of Fig. 2 displays the seasonal cycle along the equatorial band of the BLT defined by the same criteria as in Fig. 1. As expected, the BLT is significant only in the western Pacific and barely extends east of the date line. The largest values (around 20 m) occur west of the date line during the boreal winter. The variability in the west exhibits a clear annual cycle. The relationship between a significant BLT and the warmest waters ($>$28.5°C) is also evident in Fig. 2, in agreement with recent observations reported in Delcroix and McPhaden (2002). The eastward displacement of the barrier layer in boreal winter is associated with strong

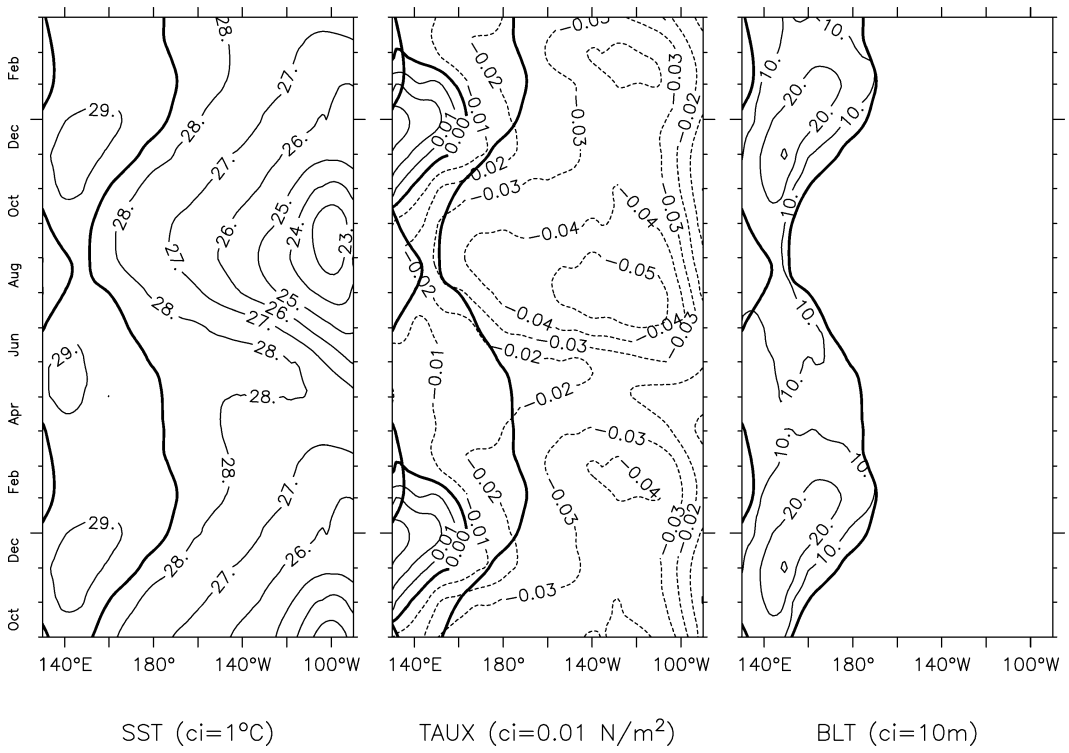

FIG. 2. Time–longitude sections averaged between 2°N and 2°S of the seasonal cycle simulated by the coupled model for SST, surface zonal wind stress, and barrier layer thickness. The thick black line represents the 28.5°C SST isotherm. The contour interval is set to 1°C, 0.01 N m^{-2}, and 10 m.

eastward currents generated by WWBs. This behavior is consistent with the present understanding of barrier layer formation along the equator (Roemmich et al. 1994; Vialard and Delecluse 1998; Cronin and McPhaden 2002). The eastern edge of the warm waters is also characterized by a strong sea surface salinity (SSS) front (not shown) that exhibits an ENSO-related variability in agreement with the results of Picaut et al. (1996) and Delcroix and Picaut (1998). Along the equator, the simulated SSS, with typical mean values less than 33.5 psu in the far western Pacific and around 35 psu in the central Pacific, presents a ''fresh'' bias as compared to the observed climatology (Delcroix et al. 1996). The excessive precipitation over the Maritime Continent and the weakness of the southeasterly trade winds in the central Pacific explain, in large part, these model deficiencies.

Figure 2 suggests that the main processes of the interaction between the SST and the wind are well captured by the model at seasonal time scales. Nevertheless, this does not guarantee that the level of interannual variability will be satisfactory (e.g., Mechoso et al. 1995). Maes et al. (2002b) have already noted the weak amplitude of typical indices such as the Southern Oscillation index (SOI) and SST anomalies in the Niño-3.4 box (5°N–5°S, 120°–170°W) in the central Pacific. However, the time series of such indices shows that the present model is able to reproduce ENSO events of different amplitudes characterized by a spectral peak at around 4 years, in agreement with observations. Most importantly, the level of interannual variability in SST is closely related to the wind stress anomalies. For example, the ratio between the variance of these variables is within 20% of the value derived from observations in the central Pacific by Davey et al. (2002).

3. Relationships between the buildup, the barrier layer, and El Niño

a. Buildup and barrier layer in the control experiment

The idea that the BLT could have a specific role during the buildup year prior to El Niño derives mainly from the observational analyses shown in Fig. 1. It is therefore important to verify that such a relationship is reproduced in the coupled model. Figure 3 displays similar time–longitude plots along the equatorial band for the SST anomaly, the 0–500-dbar thermosteric anomalies and the BLT. The period shown in Fig. 3 is restricted to the few years characterized by a strong El Niño. The mature phase of this event occurs during year 16 with a strong reduction of the equatorial upwelling in the central–eastern Pacific. The SST anomalies increase up to 4°C and warm waters above 28.5°C are present along almost all the equatorial band from March

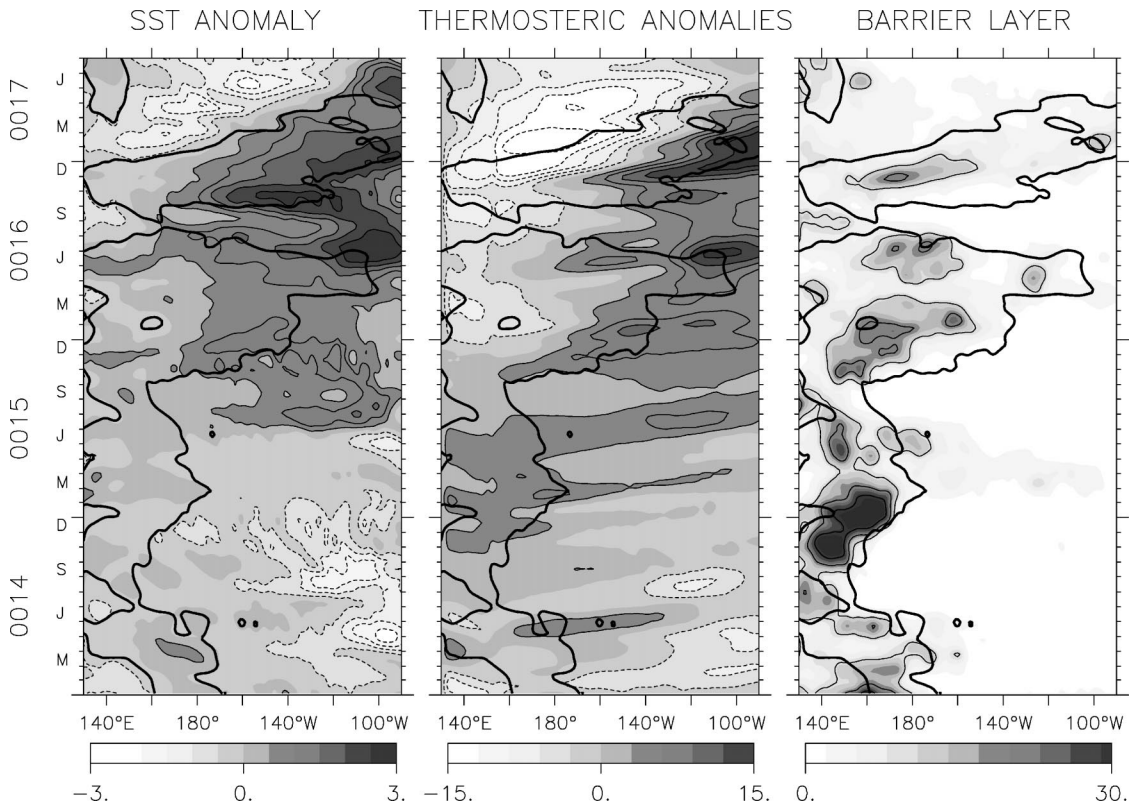

FIG. 3. Time–longitude sections averaged between 2°N and 2°S of SST anomalies, thermosteric anomalies referenced to 500 dbar, and barrier layer thickness simulated by the coupled model during years 14 to 17. The thick black line represents the 28.5°C SST isotherm. The contour interval is set to 0.5°C, 3 dyn cm, and 10 m. Dashed contours correspond to negative values.

to June. By midsummer of year 16, a slight resurgence of the seasonal upwelling reduces the warm anomalies that last, nevertheless, until the summer of year 17. Figure 3 shows that warm SST anomalies were already present since the middle of year 15 along the equatorial band. On the other hand, the spreading of the warm waters toward the central Pacific starts only at the end of that year. Most of the warm SST anomalies in the central and eastern part of the basin are associated with the arrival of downwelling equatorial Kelvin waves, as shown by the eastward propagation apparent in the thermosteric anomalies. The zonal current anomalies associated with these waves discharge the warm waters from the west into the east and, by the end of year 15, the thermosteric anomalies begin to exhibit the change in the east–west tilt of the thermocline associated with El Niño events. At this time, the warm pool reaches its easternmost position, and Fig. 3 shows that positive SST anomalies are present in the equatorial band across the entire basin. The thermosteric positive anomalies can be traced back to the start of their development in the western Pacific during the middle of year 14. During this early period of approximately one year, the entire warm pool, as defined by the 28.5°C isotherm, is characterized by positive thermosteric anomalies larger than 4 dyn cm, whereas the SST anomalies are not well defined and remain close to zero. In addition to this buildup in the western Pacific, the presence of a significant BLT is similar to the sequence shown in Fig. 1 for recently observed El Niño events.

Before testing the mechanisms linking the BLT and the heat buildup prior to El Niño, it is necessary to check that such a relationship is a robust and systematic feature of the coupled model. The SST index in the Niño-3.4 box is used as an indicator of ENSO in Fig. 4, which also displays the interannual variability of thermosteric and barrier layer anomalies over a 30-yr period. The BLT and thermosteric anomalies are averaged over the 4°N–4°S equatorial band from 130°E to the date line, a region that approximately represents the western Pacific warm pool. The time series are smoothed with a 9-month Hanning filter to focus on interannual time scales. As noted earlier, the model is able to reproduce El Niño events of different intensities and at irregular intervals of 2 to 7 years. Before each event a buildup over a time period of approximately one year is seen, but no clear relationship appears between the amplitude of the buildup and the amplitude of the following El Niño. For instance, the amplitudes of the buildups during years 10 and 14 are quite similar, whereas the intensities of the associated El Niño events are clearly different. Moreover, the presence of a buildup in this model is not a

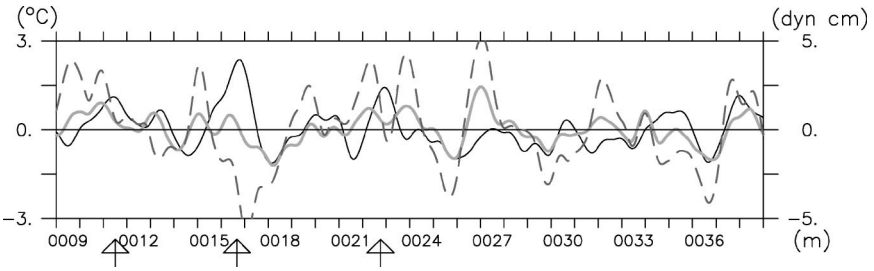

FIG. 4. Interannual evolution of the Niño-3.4 SST (black), the 0–500-dbar thermosteric (dashed), and the barrier layer thickness (gray) anomalies in the western Pacific (4°N–4°S, 130°E–180°) over a 30-yr period. The left axis corresponds to the SST index (in °C), whereas the right axis corresponds to the thermosteric anomalies (in dyn cm) and the BLT anomalies (in m).

sufficient condition to trigger El Niño. This is illustrated by the presence of a strong buildup during years 26 and 27 that was not followed by an El Niño. At best, this condition seems to be necessary. During the period prior to El Niño events, Fig. 4 shows that positive thermosteric anomalies are also associated with positive anomalies of the BLT. The amplitudes of the BLT anomalies are relatively weak, but it should be kept in mind that the BLT anomalies vary geographically and when averaged over a large region may not stand out against the background of a large seasonal signal (Fig. 2). Thus, during the months when the heat buildup occurs a significant barrier layer is already in place in the western equatorial Pacific. The relationship between the barrier layer and the heat buildup during the period prior to El Niño appears to be robust and systematic in the coupled model.

The existence of this relationship does not necessarily mean that the barrier layer plays an active role during the buildup of heat in the western Pacific. A possible physical mechanism for the importance of the barrier layer will be discussed later. To examine further the correlations between the variations in wind stress, thermosteric anomalies, and BLT, lagged correlations were calculated between these different variables on a monthly basis (Fig. 5). Interannual anomalies of the equatorial wind stress exhibit a negative correlation with the thermosteric anomalies of the western Pacific, which is maximum (−0.73, 95% significance −0.30) when negative wind stress anomalies lead positive thermosteric anomalies by 3 months. This is consistent with Wyrtki's (1975) idea that trade winds in the central equatorial Pacific cause water to pile up in the western Pacific. In the coupled model, the lagged-correlation coefficient exhibits quite similar values if the wind stress data are replaced by the averaged value between 160°E and 160°W, that is, representative of the central equatorial Pacific only. Most importantly, the negative correlation is significant over a lagged time period of about one year, in agreement with the values deduced from observations by Li and Clarke (1994).

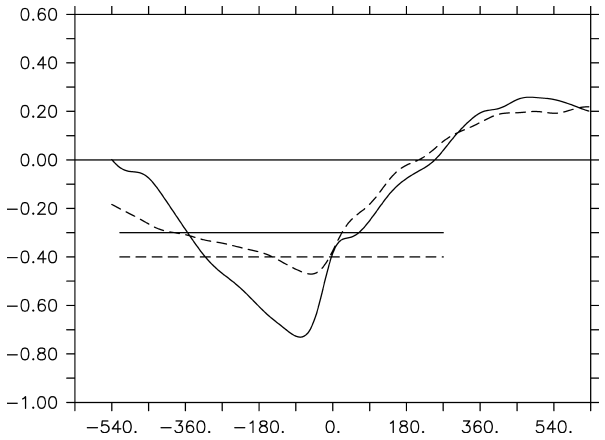

FIG. 5. Lagged-correlation coefficient between (solid line) surface equatorial zonal wind stress and thermosteric anomalies in the western Pacific and (dashed line) BLT (with a reversed sign) and thermosteric anomalies in the western Pacific. Negative lag in days means that thermosteric anomalies and BLT lags wind stress and thermosteric anomalies, respectively. The horizontal lines represent the significance at the 95% confidence level.

In order to investigate the relationship between the heat buildup and the barrier layer, a similar calculation is performed between the thermosteric anomalies and the BLT over the western Pacific. If a BLT increase corresponds mainly to a freshening of the upper layers, the correlation between the BLT and the thermosteric anomalies should be positive. This is indeed the case in Fig. 5, with a reversed sign of the BLT consistent with the previous correlation between the buildup and wind stress. The lagged correlation is maximum (−0.47; 95% significance −0.40) when the BLT leads the positive thermosteric anomalies by about 2 months. In a similar way, as the relation between the wind stress and the heat buildup, the significant correlation between the BLT and the heat buildup lasts over a period of approximately 6 months (Fig. 5). Both correlations reflect that the barrier layer is thickening at approximately the same time as the strengthening of the trade winds that sustain the buildup in the western Pacific. This does not mean that the barrier layer could be considered as another precursor of El Niño, but its potential role during the buildup represents an interesting hypothesis to be tested in the coupled model.

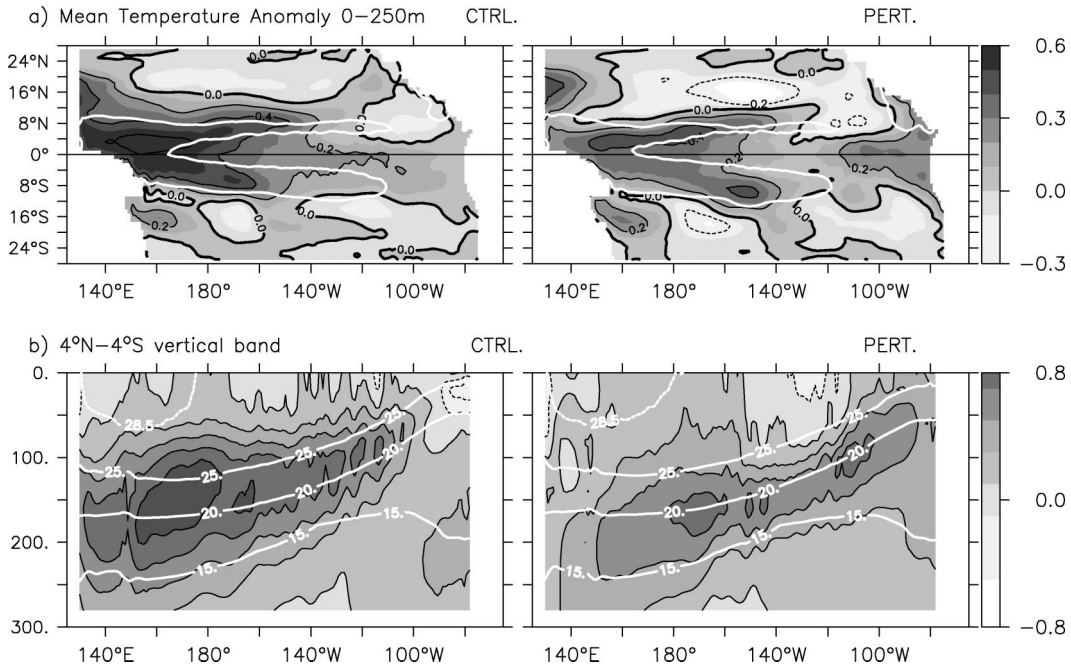

FIG. 6. (a) Difference of the 0–250-m averaged temperature (in °C) between (left) the control and (right) the perturbed experiments averaged over the buildup year vs the 30-yr climatology of the model. The white lines represent the 28.5°C SST isotherm. (b) Vertical temperature difference (in °C) averaged between 4°N and 4°S between (left) the control and (right) the perturbed experiments during the buildup year vs the 30-yr climatology of the model. The white lines are the temperature isotherms of each experiment. The contour interval is set to 0.2°C. Dashed contours correspond to negative values.

b. Reduction of the buildup prior to El Niño

In the following, the control experiment refers to the standard physics of the model as previously discussed, whereas perturbed experiments are conducted in two stages. The first stage tests the role played by the barrier layer during the heat buildup. The second stage investigates the effects of the first stage on the El Niño event that followed. In the first stage, the vertical mixing scheme in the ocean model is modified by removing its dependence on the salinity stratification as proposed by Maes et al. (2002b). Specifically, the salinity terms are removed from the McDougall (1987) formulation of the Brunt–Väisälä frequency, N^2, as it appears in the mixing scheme. In the warm pool region, the effect is to decrease N^2 and increase the vertical mixing coefficient at the depth of the barrier layer. The resulting increase of vertical mixing destroys, or significantly reduces, the salinity stratification on which the barrier layer relies. Since the focus is on the heat buildup in the equatorial warm pool, the modifications were made only in the 4°N–4°S band and only in areas where SST is warmer than or equal to 28°C. This procedure guarantees that the entire signal of the BLT of the western Pacific is affected (see Figs. 2 and 3). In the second stage, the salinity stratification influence on N^2 is restored and the model is restarted using the state reached at the end of the first stage as initial conditions.

One important question concerns the timing of the two stages in the perturbed experiment; that is, when do these modifications have to start and stop to ensure the removal of the barrier layer and thus allow the absence of the barrier layer to have a possible effect on the heat buildup? In Figs. 4 and 5, the heat buildup is maximal a few months to a year prior to the mature phase of an El Niño event. The increase in the BLT also leads this maximum by a few months, so the modifications to the mixing scheme were applied for a period of one year prior to the onset of the event. For the perturbed replay of the strong El Niño displayed in Fig. 3, the first stage is started in October of year 14. This date also corresponds to a time when the warm pool is in its westernmost position, and thus it minimizes the initial shock in the coupled model. At the end of the 1-yr period, the normal formulation of the mixing scheme is restored and the second stage of the perturbed experiment is run for a period of 18 months in order to analyze the impact of the reduced BLT and the modified heat buildup on El Niño.

The annual mean differences during the buildup year are first discussed here, while the time evolution of these differences is presented in section 4. As expected, the BLT is reduced within 2–3 months of the start of the perturbed experiment and does not significantly reappear within the western equatorial Pacific during the first stage. Figure 6a displays for the tropical Pacific Ocean the difference in the average temperature of the

top 250 m between the buildup year and the 30-yr climatology of the model. It must be kept in mind that the region where the modified mixing scheme is applied only represents a band of 40° of longitude from the western boundary to the date line and of 8° of latitude as shown by the 28.5°C SST isotherm superimposed on Fig. 6a. Within the 4°N–4°S band, the Pacific heat buildup in both the control and perturbed experiments is characterized by a positive anomaly, but there are significant differences between the two experiments. In the western Pacific the anomaly of 0.5°C in the control experiment is reduced by a factor of 2 or more in the perturbed experiment, while in the eastern part of the basin a positive anomaly of 0.2°C appears that is not present in the control experiment. This result suggests that there is a shift of the heat buildup from the western to the eastern equatorial Pacific during that period of time in the perturbed experiment. Moreover, the net surface heat flux in the eastern Pacific is lower in the perturbed experiment compared to the control experiment (around -10 W m^{-2} in the cold tongue). This point indicates a dynamical rather than a thermodynamical origin for the heat buildup differences. Large negative anomalies appear in the upper-ocean temperature of the perturbed experiment in the central and western Pacific of the Northern and Southern Hemispheres, respectively. These differences are correlated with the differences in wind stress curl (not shown), which also suggests a dynamical response of the ocean.

To complete this spatial description, it is important to locate the main differences as a function of depth. Both the main thermocline as defined by the waters between 15° and 25°C and the temperature anomaly over the 4°N–4°S band are represented in Fig. 6b. If the surface exhibits some differences such as a more pronounced cooling in the central Pacific in the perturbed experiment, it is obvious that the main differences are located within the thermocline. In the western Pacific between the western boundary and the date line, the temperature within the thermocline decreases from values greater than 1°C in the control experiment to 0.5°C in the perturbed experiment. In contrast, the changes in the upper layers (i.e., the warm pool) are relatively weak with mostly an extension of the warm waters toward the central part (see also Fig. 6a). In the central Pacific, the temperature decreases slightly, while in the eastern Pacific it increases up to 0.5°C near the coast in the perturbed experiment, replacing the slightly negative anomaly of the control experiment. Note that the perturbed experiment is closer to normal seasonal conditions than it is to the control experiment.

c. Annihilation of the strong El Niño

Figure 6 shows a reduction of the heat buildup prior to the onset of the strong El Niño in the perturbed experiment, but is this reduction large enough to have an impact on the development of El Niño? This question merits a careful response because heat buildups similar to or weaker than the one reproduced in the perturbed experiment can be associated with a warm event. The sequence from years 33 to 35 illustrates one such example in the control experiment (Fig. 4). To investigate fairly the impact of the modified heat buildup it is necessary to generate ensembles of both the control and perturbed experiments starting in October of year 15. This is done because it is well known that the internal variability of the Tropics is strong enough to disrupt the onset of El Niño through nonlinear processes. Six-member ensembles were produced for each experiment by introducing small random perturbations [$O(0.1°C)$] in the initial conditions of the SST over the warm pool region. In the control ensemble, the SST perturbations are applied once. In the perturbed ensemble, the final states obtained at the end of the first stage, as discussed in the previous section, are used as initial conditions for the second stage. Thus in the perturbed simulations, the same SST perturbations as applied in the control ensemble are applied at the start of the second stage. The experiments are performed up to the middle of year 17 in order to encompass the mature phase of the strong El Niño (Fig. 3). The response of each experiment is examined through the behavior of three parameters: SST, zonal wind stress, and 0–500-dbar thermosteric anomalies over the 4°N–4°S band. The anomalies are averaged during year 16 corresponding to the mature phase of the original event and are displayed in Fig. 7 for each ensemble.

In the control ensemble, four of the six experiments result in a strong El Niño with typical SST anomalies in the central–eastern part of the basin warmer than 1°C during year 16. Associated with these warm anomalies, westerly wind anomalies are well developed in the central Pacific, west of the SST anomalies. In the subsurface, the east–west tilt of the thermosteric anomalies flattens in both western and eastern parts of the basin (Fig. 7c). These features depict the mature phase of a relatively well-developed El Niño. In the perturbed ensemble, although the barrier layer recovers quickly in stage two, typically in less than 15 days, the positive SST anomalies associated with El Niño disappear. Their amplitude is generally less than 0.5°C throughout the equatorial band, with some members of the ensemble exhibiting slightly cold anomalies (Fig. 7a). Consistent with the absence of El Niño, the wind stress does not show westerly anomalies over the equatorial band, except in the far western Pacific, which is still characterized by the presence of WWBs in the perturbed experiments. East of the date line, the ensemble average of the wind stress anomaly is close to zero, indicating a return to the seasonal cycle of the model. As for the thermosteric anomalies, they remain slightly positive but constant all over the entire equatorial band. The remaining heat buildup from the first stage of the perturbed experiment does not evolve and no heat or mass transfer from the west to the east appears during the

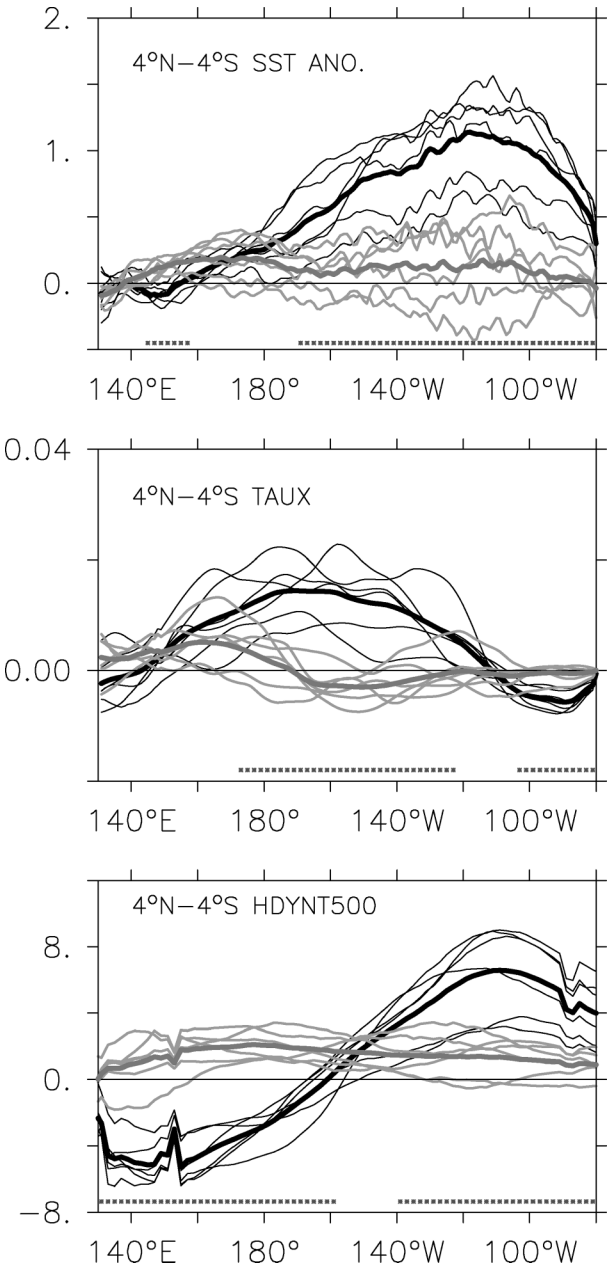

FIG. 7. Annual mean anomaly of year 16 averaged between 4°N and 4°S of (a) SST, (b) surface zonal wind stress, and (c) 0–500-dbar thermosteric anomalies as a function of longitude. The thin black lines correspond to the control ensemble whereas the thin gray lines correspond to the perturbed ensemble. The thick lines represent the ensemble mean. The square dot line at the bottom of each panel indicates where the difference between the two ensembles is significant at the 95% confidence level.

second stage of the perturbed experiment. The differences between the two ensembles are robust and are statistically significant at the 95% confidence level as shown in the bottom of each panel (Fig. 7). Hence, the reduction of the buildup due to the removal of the barrier layer during the year prior to the event can be clearly associated with the annihilation of the strong El Niño. Similar conclusions can be drawn from tests for other El Niño events and will be discussed in section 5.

4. Physical mechanisms of the heat buildup–BLT relationship

The systematic disappearance of El Niño conditions following the reduction of the heat buildup highlights the importance of its relationship with the barrier layer during the preceding year, but it also raises some questions about the physical mechanisms at work. It should be kept in mind that, although the modifications are applied only in the equatorial western Pacific, the response is basinwide.

Figure 8 exhibits the response of the model for both control and perturbed experiments during the 1-yr period when the modifications to the mixing scheme were applied. The SST field, the zonal wind stress, and the anomaly of the 20°C isotherm depth are displayed together with the 34.25-psu surface isohaline (white line). The 20°C depth anomaly is used to summarize the thermocline behavior but it is also strongly related to the heat content and to the sea level (e.g., Rebert et al. 1985). The 34.25-psu SSS value represents a useful way to identify the salinity front, which is associated with the zonal displacements of the eastern edge of the warm pool (Picaut et al. 1996). Hereafter, the term ''warm pool'' will refer to the region extending from the western boundary to the longitudinal position of this SSS value. In the control experiment, a series of WWBs appears over the warm pool from November of year 14 to the end of April of year 15 (Fig. 8, top). These westerly winds maintain locally the warm SSTs through Ekman convergence in the upper layers and the generation of downwelling equatorial Kelvin waves. The propagation of the Kelvin waves is shown in the 20°C depth anomaly. If the first series of WWBs results in an eastward displacement of the warm pool, only the waves associated with the second series in January–February of year 15 significantly depress the thermocline and propagate to the eastern part of the basin by April. At that time, positive thermosteric anomalies have already spread throughout the entire equatorial band (Fig. 3). The Kelvin waves associated with the third series of WWBs in late April of year 15 maintain the depression of the thermocline, but more importantly, they arrive in July–August at the beginning of the upwelling season in the east (Fig. 2). Figure 3 shows that this period corresponds to the switch from negative to positive SST anomalies. Around this period, the equatorial band is fully charged and the conditions are favorable for the development of a warm event during the next boreal winter. In the control experiment, the development of such conditions is clearly associated with the generation and timing of downwelling equatorial Kelvin waves.

In the perturbed experiment (Fig. 8, bottom), the relationship between the heat buildup, the Kelvin waves,

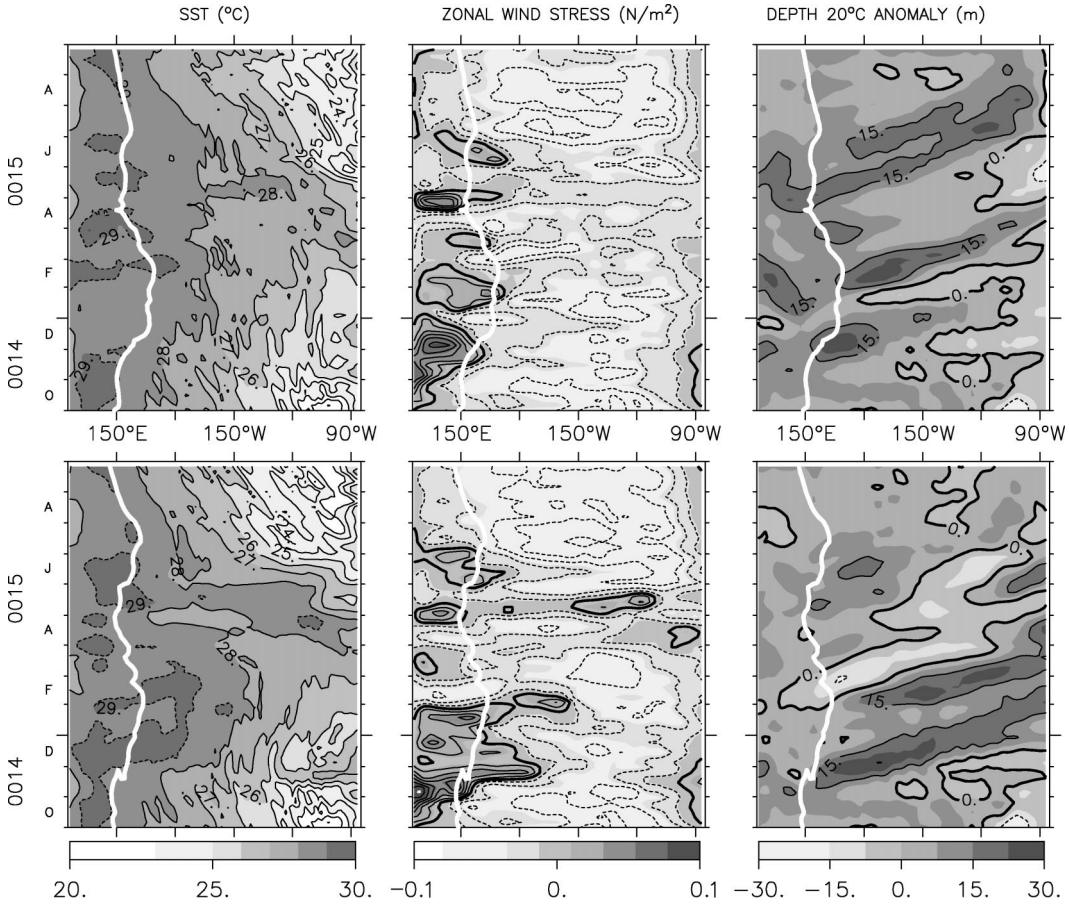

FIG. 8. Time–longitude sections averaged between 2°N and 2°S of SST, surface zonal wind stress, and 20°C depth anomaly in the (top) control and (bottom) perturbed experiments during the 1-yr period (14 Oct–15 Sep). The thick white line is the 34.25 SSS value. (top left) The 29°C isotherm corresponds to the dashed line whereas positive, negative, and zero contours of the zonal wind stress and of the 20°C depth anomaly are, respectively, represented by solid, dashed, and thick lines. The contour interval is respectively set to 1°C, 0.01 N m^{-2}, and 10 m. Dashed contours correspond to negative values.

and the seasonal cycle is clearly different, especially in the central and eastern part of the basin. The period from October of year 14 to January of year 15 is still characterized by a series of WWBs over the warm pool but, while the intensity of the bursts is similar to the control experiment, the fetch of the WWBs extends farther along the equator. In November of year 14 for instance, westerly winds blow over the western Pacific out to the date line, a limit that is far beyond the eastern edge of the warm pool. It should be noted that the eastward displacement of the warm pool itself is not significantly different when compared to the control experiment. Within the warm pool, it takes less than 3 months to suppress the positive anomalies in the 20°C depth isotherm, and the absence of variability in these anomalies indicates that the seasonal conditions prevail during the rest of the perturbed experiment. Associated with the different wind stress conditions, the response of the ocean is different as well in the central and eastern parts of the basin. Downwelling equatorial Kelvin waves are generated earlier in the year and due to the extended wind fetch they propagate throughout the equatorial band. By the end of January of year 15, the thermocline has been depressed by 10–20 m in the eastern Pacific. At the end of April the heat buildup is mostly gone and it will not recover. A few WWBs still appear in March and April, but it is clear that they do not generate strong Kelvin waves and, consequently, they do not influence the central and eastern Pacific. Compared to the control experiment, the timing of the Kelvin waves is different in the perturbed experiments and the coincidence of their arrival with the development of the upwelling season is not so marked. Starting in July of year 15, the upwelling season in the perturbed experiment is more pronounced (Fig. 8, left) and closer to the mean seasonal conditions in terms of westward extension and intensity than in the control experiment (Fig. 2). These contrasting results suggest that the sensitivity of the coupled response to the removal of the barrier layer is strongest from October to March and that the dynamics of the

TABLE 1. Averaged values of SST, barrier layer thickness, mixed layer depth (MLD), and momentum supply by the zonal wind stress over the warm pool and eastern edge regions (see the text for definitions) for the control and perturbed experiments from Oct to Dec of year 14, prior to El Niño.

	Warm pool		Eastern edge	
	Control	Perturbed	Control	Perturbed
SST (°C)	28.9	29.0	28.3	28.6
BLT (m)	46.0	17.0	7.4	7.4
MLD (m)	38.0	57.0	54.0	52.0
$u\tau_x$ (N m^{-1} s^{-1})	0.32	0.96	0.78	0.73

TABLE 2. Averaged values of the major terms implied in the mixed layer heat budget over the warm pool and eastern edge regions (see the text for definitions) for the control and perturbed experiments from Oct to Dec of year 14, prior to El Niño. The units are in °C month^{-1}.

Mixed layer budget (in °C month^{-1})	Warm pool		Eastern edge	
	Control	Perturbed	Control	Perturbed
Tendency	0.34	0.10	0.30	0.42
Advection	0.28	0.20	0.02	0.14
Atmospheric forcing	−0.06	0.28	0.67	0.64
Entrainment	0.12	−0.38	−0.41	−0.36

warm pool has an important influence during this period. It justifies a posteriori the choice of the 1-yr period for the first stage of the perturbed experiment in order to test the effects of the heat buildup–BLT relationship on the development of El Niño.

Figure 8 shows that the series of WWBs in the perturbed experiment is associated with the presence of SSTs warmer than 29°C within and beyond the warm pool. In order to investigate these SST differences, the heat budget of the mixed layer in two regions of the 2°N–2°S band is considered. The first region is the warm pool as defined by the 34.25-psu SSS criterion previously mentioned; the second region is located in the east of the warm pool and extends 25° eastward from the 34.25-psu isohaline. Tables 1 and 2 give different parameters of interest averaged over these two regions from October to December of year 14. For the mixed layer heat budget, the methodology consists of integrating separately the terms in the equation of temperature over the time-variable depth of the mixed layer. The total tendency of the budget results from the contributions of the horizontal and vertical advections, the combined effect of shortwave radiation and surface heat flux (referred to hereafter as atmospheric forcing), and the entrainment of water from below associated with the turbulent mixing of heat. The horizontal diffusion always represents a sink of heat, but its amplitude remains negligible when compared to the dominant terms.

In the warm pool region of the perturbed experiment, the BLT is reduced by a factor of 3 and the mixed layer depth consequently increases (Table 1). As expected, the reduction of the BLT induces a strong modification of the vertical heat transfer. In the control experiment, the water parcels exchanged at the bottom of the mixed layer have the same or an even warmer temperature, resulting in a positive source for the heat budget. In the perturbed experiment, the entrainment cooling of the mixed layer is operative and becomes the dominant term of the heat budget (Table 2). The process that opposes this cooling is provided by the atmospheric heating, which acts as a thermostat (0.28 against −0.38). The positive contribution of the atmosphere is linked to the increase in depth of the mixed layer that is thus able to gain more solar heat flux. It is also related to the importance of the atmospheric convection over the warm pool. The projection of wind stress over a deepening mixed layer results in reduced surface currents and a slight reduction in the advective contribution to the heat budget. Finally, although the total tendency of the heat content is reduced due to the deepening of the mixed layer, it remains positive, and this largely explains the presence of anomalously warm SST in the perturbed experiment (Fig. 8; Table 1).

Tables 1 and 2 show that quite similar dynamics operate in the eastern region for both the perturbed and control experiments. The differences are small and are related to the dynamics of the warm pool. For instance, the SST is slightly larger in the perturbed experiment and it results mainly from the stronger contribution of advection to the mixed layer heat budget. The main terms of the advection are the zonal and meridional components, and their amplitudes are related to the stronger zonal fetch of the wind initiated over the warm pool. The larger fetch of the wind, resulting from its coupling with the warm SST, induces a larger momentum supply into the ocean (Table 1). This coupling induces not only a local response in the convective activity of the atmosphere but also a response in the planetary-scale divergent circulation. In the perturbed experiment, the strong convective center is displaced eastward by 20° to 40° of longitude compared to the control experiment and explains the positive equatorial differences near the date line region shown in Fig. 9. In this region, this corresponds to a difference of order to 30% in the 1000-hPa potential velocity field.

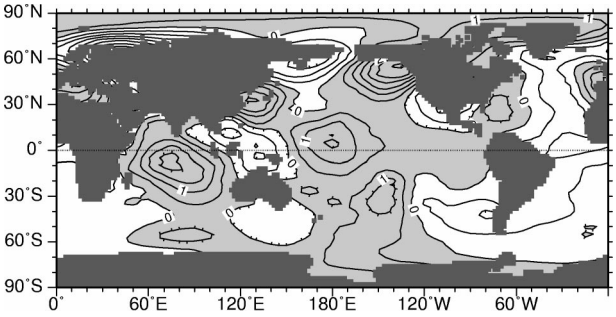

FIG. 9. Global differences of the 1000-hPa potential velocity (in 10^6 m^2 s^{-1}) between the perturbed vs the control experiments during the Oct–Dec period of year 14. Positive differences are shaded.

5. Discussion and conclusions

These analyses of oceanic and atmospheric responses to the removal of the barrier layer in the coupled model confirm the importance of the warm pool dynamics for El Niño. The switching on or off of the entrainment cooling associated with the barrier layer is responsible for mixed layer changes that, in return, control SST changes. The high sensitivity of the atmospheric response to small SST changes over the warm pool results in local and basin scale oceanic responses. During the particular period of heat buildup, the deepening of the mixed layer associated with the removal of the barrier layer and the net surface heat flux results in the maintenance of warm SST. It favors the subsequent zonal extension of the fetch of the WWBs. The enhanced vertical mixing below the mixed layer dissipates one part of the heat buildup in the western Pacific, whereas downwelling Kelvin waves generated by WWBs insure the discharge of the remaining excess of heat toward the eastern Pacific. The failure of El Niño to develop also confirms the necessary condition of the heat buildup for the development of El Niño.

Our presentation so far has focused on a particular El Niño in order to detail the physical mechanisms at work. It is necessary to examine similar experiments on other El Niño events in order to gain confidence in the results and to isolate the most important features. The El Niño events of year 11 and year 22, as indicated by the arrows in the bottom of Fig. 4, may be useful in this regard. These events are characterized by different intensities and by different preconditions, as compared to the strong event of year 16 (Fig. 4). For example, while the warm event of year 22 is also preceded by a cold event, the buildup prior to the event of year 11 is a period of near-zero SST anomaly. These two El Niño events were explored by means of perturbed experiments with mixing scheme modifications during a first stage covering, respectively, the 09/10–10/10 and 20/10–21/10 one-year periods. During these periods, the BLT in the western Pacific in the control experiment is smaller with values around 35 m as compared to 46 m for the strong event. Nevertheless, the different mechanisms at work during both perturbed experiments are not fundamentally changed. The net result of removing the barrier layer's influence on vertical mixing is to reduce the heat buildup by a factor of 2 to 4 in the western Pacific and to discharge the heat toward the eastern Pacific before the onset of El Niño. This decrease occurs in the thermocline of the equatorial band. The increase in the mixed layer depth, the maintenance or even slightly increase of warm SST within and eastward of the warm pool, as well as the thermostat role of the atmosphere are also confirmed. The coupled response of the warm pool is characterized by a wind fetch extension that generates a remote response in the rest of the basin, through downwelling equatorial Kelvin waves. At the end of each buildup period (i.e., the first step of the perturbed experiments), six-member ensembles are generated following the same methodology as discussed in the strong El Niño (section 3c). The annual mean SST anomaly along the equator for each ensemble, control and perturbed, is displayed in Fig. 10. For both El Niño events (years 11 and 22), the mean difference is significant over most of the central and eastern equatorial band. Three members of the perturbed ensemble for year 11 do show some warm anomalies associated with an east–west tilting of the thermocline (not shown). These three members, as well as one member associated with the perturbed ensemble of the strong event (Fig. 7), have a mean SST anomaly larger than 0.5°C. These four members could be thus identified as El Niño events. However, these 4 members are a small fraction of the total of 18 members, and the suppression of the warm events due to the modifications of the relationship between the heat buildup and the BLT is considered to be significant.

It is important to use fully coupled models to explore

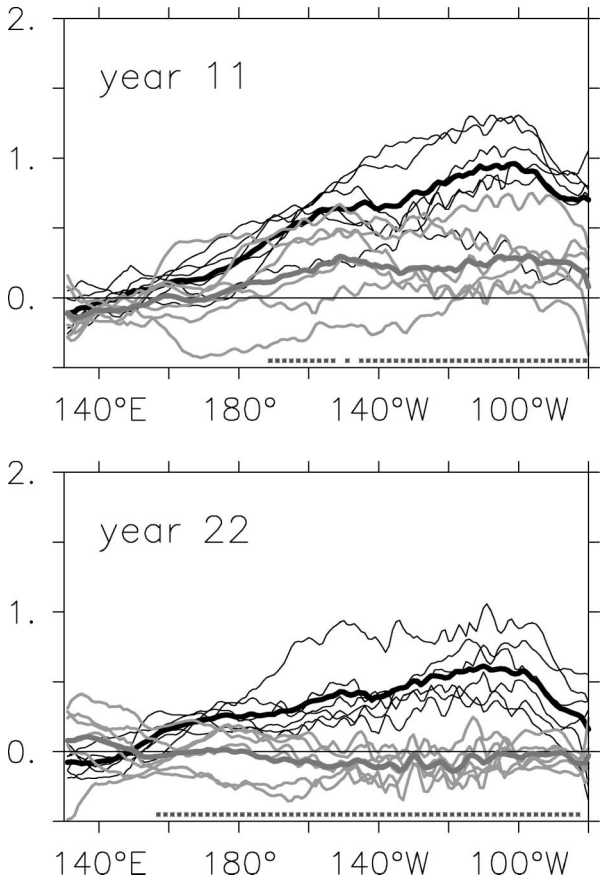

FIG. 10. Annual mean anomaly averaged between 4°N and 4°S of SST for (top) year 11 and (bottom) year 22 as a function of longitude. The thin black lines correspond to the control ensemble whereas the thin gray lines correspond to the perturbed ensemble. The thick lines represent the ensemble mean. The square dot line at the bottom of each panel indicates where the difference between the two ensembles is significant at the 95% confidence level.

the feedbacks between the barrier layer, the mixed layer, and the SST. Maes et al. (2002b) have recently investigated the impact of the barrier layer on the onset of El Niño through similar perturbed experiments. In both that study and the present one the barrier layer was removed, enabling entrainment cooling and deepening of the mixed layer. However, the timing and duration of the perturbed stages of the experiments were chosen differently in these two studies. In Maes et al. (2002b), the removal of the barrier layer was done during the series of WWBs just before the onset of El Niño (starting in October of year 15) whereas, in the present study, this removing is done during the 1-yr buildup period prior to the onset of El Niño (from October of year 14 to September of year 15). The results show different effects on the heat budget of the mixed layer and on the SST. Maes et al. (2002b) reported a slight decrease in the warm SST as compared to the maintenance of the warm SST of the warm pool in the present study. This difference in SST is mainly explained by the difference in the westerly wind fetch and in the overall response of the coupled system at the basinwide scale. Because of this sensitivity to the timing of the presence of the barrier layer, it would be worthwhile to conduct similar barrier layer experiments with other coupled models, which may have different mean states and different levels of interannual variability.

An understanding of processes that regulate SST in the western equatorial Pacific was one major motivation of the 1992–93 Coupled Ocean–Atmosphere Response Experiment (COARE). On the list of potential feedbacks that were uncertain at the time of the COARE implementation, Webster and Lukas (1992) mentioned the possibility that the salinity barrier layer processes could provide a long-term memory mechanism between El Niño events. The present study offers a variation on that idea in that it establishes a precise role for the barrier layer in the heat buildup prior to El Niño events.

As previously stated, the relationship between the heat buildup and the barrier layer appears to be a necessary condition to maintain the heat buildup in the equatorial Pacific over a 1-yr period. The heat buildup then provides the potential for an El Niño to develop. Of course, it does not establish that the relationship is sufficient because other processes could also be necessary for SST changes in the warm pool independent of the barrier layer effects. In order to evaluate the importance of the barrier layer in the intrinsic variability of the system, an additional experiment was performed. The modifications in the vertical mixing scheme were applied in the same manner, that is, in the 4°N–4°S band and over waters warmer or equal to 28°C, but they were continuously applied during a 30-yr period. This simulation exhibits a mean state and a seasonal cycle similar to those in the control experiment, but it also supports a weak ENSO variability. It suggests the idea that the heat buildup–salinity barrier layer relationship is not a sufficient condition for El Niño, but it also seems to suggest that this condition is not necessary either. A closer look at the results of the additional experiment can resolve the apparent contradiction. Recall that the modifications in the vertical mixing scheme used in the present study can only begin to reduce or to remove the barrier layer once it has been formed. Some residual BLT values of about 10 m are present in this additional simulation and they persist for a few weeks before being destroyed. This short period represents, however, a sufficient time to sustain the heat buildup in the western central Pacific, so the model can develop weak to moderate El Niño events. To further extend the analysis of the role of the barrier layer, it will be important to fully consider the mechanisms that lead to its formation such as discussed by Roemmich et al. (1994) and Cronin and McPhaden (2002). The coupled response of the Pacific Ocean in a simulation where one or several of such mechanisms are suppressed has not yet been explored and further investigations are required.

To conclude, there is more and more evidence that the salinity barrier layer plays an important role in the dynamics of El Niño. The relationship between the heat buildup and the barrier layer over long periods of time represents a necessary condition for a sustained accumulation of heat in the western Pacific. In this region, the heat buildup is a direct consequence of the suppression of the entrainment cooling below the mixed layer due to the presence of the barrier layer. The subsequent development of El Niño in the central and eastern equatorial band is the remote response to Kelvin waves generated by the SST–wind coupling over the warm pool. The removal of the barrier layer in the western Pacific causes the reduction and discharge of the heat buildup in the western Pacific before the onset of El Niño and thus prevents the development of El Niño. These results are an argument for the development of real-time in situ observations of the barrier layer both for assessing the applicability of these results and potentially for providing observations to initialize El Niño forecasts.

Acknowledgments. The authors would like to thank the French community in charge of the LODYC/Météo-France coupled model. Computer facilities were provided by Météo-France and by the Centre National d'Etudes Spatiales. We would also like to thank Dave Behringer, Thierry Delcroix, and Gérard Eldin, as well as the two anonymous reviewers, for their comments. This work was supported by an ''Action Thématique Innovante'' funded by the Institut National des Sciences de l'Univers, by the Programme National d'Etudes de la Dynamique du Climat, and by the Institut de Recherche pour le Développement.

REFERENCES

Ando, K., and M. J. McPhaden, 1997: Variability of surface layer hydrography in the tropical Pacific Ocean. *J. Geophys. Res.*, **102,** 23 063–23 078.

Battisti, D. S., and A. C. Hirst, 1989: Interannual variability in a tropical atmosphere–ocean model: Influence of the basic state, ocean geometry and nonlinearity. *J. Atmos. Sci.,* **46,** 1687–1712.

Belamari, S., 2002: Etude du rôle des coups de vent d'ouest dans le déclenchement d'évènements chauds de type El Niño. Ph.D. thesis, Université Paul Sabatier, Toulouse, France, 236 pp.

——, J.-L. Redelsperger, and M. Pontaud, 2003: Dynamic role of a westerly wind burst in triggering an equatorial Pacific warm event. *J. Climate,* **16,** 1869–1890.

Bjerknes, J., 1969: Atmospheric teleconnections from the equatorial Pacific. *Mon. Wea. Rev.,* **97,** 163–172.

Blanke, B., and P. Delecluse, 1993: Variability of the tropical Atlantic Ocean simulated by a general circulation model with two different mixed layer physics. *J. Phys. Oceanogr.,* **23,** 1363–1388.

Bougeault, P., 1985: A simple parametrization of the large-scale effects of deep cumulus convection. *Mon. Wea. Rev.,* **113,** 2108–2121.

Cane, M. A., and S. E. Zebiak, 1985: A theory for El Niño and the Southern Oscillation. *Science,* **228,** 1085–1087.

Cronin, M. F., and M. J. McPhaden, 2002: Barrier layer formation during westerly wind bursts. *J. Geophys. Res.,* **107,** 8020, doi: 10.1029/2001JC001171.

Davey, M. K., and Coauthors, 2002: STOIC: A study of coupled model climatology and variability in tropical ocean regions. *Climate Dyn.,* **18,** 403–420.

Delcroix, T., and J. Picaut, 1998: Zonal displacement of the western equatorial Pacific ''fresh pool.'' *J. Geophys. Res.,* **103,** 1087–1098.

——, and M. McPhaden, 2002: Interannual sea surface salinity and temperature changes in the western Pacific warm pool during 1992–2000. *J. Geophys. Res.,* **107,** 8002, doi:10.1029/2001JC000862.

——, C. Hénin, V. Porte, and P. Arkin, 1996: Precipitation and sea surface salinity in the tropical Pacific Ocean. *Deep-Sea Res.,* **43A,** 1123–1141.

Déqué, M., C. Dreveton, A. Braun, and D. Cariolle, 1994: The ARPEGE/IFS atmosphere model: A contribution to the French community climate modelling. *Climate Dyn.,* **10,** 249–266.

Geleyn, J.-F., 1987: Use of a modified Richardson number for parameterizing the effects of shallow convection. *Short- and Medium-Range Numerical Weather Prediction,* T. Matsuno, Ed., Meteorological Society of Japan, 141–149.

Jin, F.-F., 1997a: An equatorial ocean recharge paradigm for ENSO. Part I: Conceptual model. *J. Atmos. Sci.,* **54,** 811–829.

——, 1997b: An equatorial ocean recharge paradigm for ENSO. Part II: A stripped down coupled model. *J. Atmos. Sci.,* **54,** 830–846.

Latif, M., and M. Flügel, 1991: An investigation of short-range climate predictability in the tropical Pacific. *J. Geophys. Res.,* **96,** 2661–2673.

Levitus, S., 1982: *Climatological Atlas of the World Ocean.* NOAA Prof. Paper 13, 173 pp. and 17 microfiche.

Li, B., and A. J. Clarke, 1994: An examination of some ENSO mechanisms using interannual sea level at the eastern and western equatorial boundaries and the zonally averaged equatorial wind. *J. Phys. Oceanogr.,* **24,** 681–690.

Lindstrom, E., R. Lukas, R. Fine, E. Firing, S. Godfrey, G. Meyers, and M. Tsuchiya, 1987: The Western Equatorial Pacific Ocean Circulation Study. *Nature,* **330,** 533–537.

Lukas, R., and E. Lindstrom, 1991: The mixed layer of the western equatorial Pacific Ocean. *J. Geophys. Res.,* **96,** 3343–3357.

Madec, G., P. Delecluse, M. Imbard, and C. Lévy, 1998: OPA 8.1 Ocean General Circulation model reference manual. Note du Pôle de modélisation Institut Pierre-Simon Laplace 11, 91 pp.

Maes, C., and D. Behringer, 2000: Using satellite-derived sea level and temperature profiles for determining the salinity variability: A new approach. *J. Geophys. Res.,* **105,** 8537–8547.

——, G. Madec, and P. Delecluse, 1997: Sensitivity of an equatorial Pacific OGCM to the lateral diffusion. *Mon. Wea. Rev.,* **125,** 958–971.

——, M. J. McPhaden, and D. Behringer, 2002a: Signatures of salinity variability in tropical Pacific Ocean dynamic height anomalies. *J. Geophys. Res.,* **107,** 8012, doi:10.1029/2000JC000737.

——, J. Picaut, and S. Belamari, 2002b: Salinity barrier layer and onset of El Niño in a Pacific coupled model. *Geophys. Res. Lett.,* **29,** 2206, doi:10.1029/2002GL016029.

McDougall, T. J., 1987: Neutral surfaces. *J. Phys. Oceanogr.,* **17,** 1950–1964.

Mechoso, C. R., and Coauthors, 1995: The seasonal cycle over the tropical Pacific in coupled ocean–atmosphere general circulation models. *Mon. Wea. Rev.,* **123,** 2825–2838.

Meinen, C., and M. J. McPhaden, 2000: Observations of warm water volume changes in the equatorial Pacific and their relationship to the El Niño and La Niña. *J. Climate,* **13,** 3551–3559.

Morcrette, J.-J., 1990: Impact of changes to the radiation transfer parameterizations plus cloud optical properties in the ECMWF model. *Mon. Wea. Rev.,* **118,** 847–873.

Perigaud, C., and C. Cassou, 2000: Importance of oceanic decadal trends and westerly wind bursts for forecasting El Niño. *Geophys. Res. Lett.,* **27,** 389–392.

Picaut, J., M. Ioualalen, C. Menkes, T. Delcroix, and M. J. McPhaden, 1996: Mechanism of the zonal displacements of the Pacific warm pool: Implications for ENSO. *Science,* **274,** 1486–1489.

Rebert, J.-P., J.-R. Donguy, G. Eldin, and K. Wyrtki, 1985: Relations between sea level, thermocline depth, heat content, and dynamic height in the tropical Pacific Ocean. *J. Geophys. Res.,* **90,** 11 719–11 725.

Reynolds, R. W., and T. M. Smith, 1995: A high-resolution global sea surface temperature climatology. *J. Climate,* **8,** 1571–1583.

Roemmich, D., M. Morris, W. R. Young, and J.-R. Donguy, 1994: Fresh equatorial jets. *J. Phys. Oceanogr.,* **24,** 540–558.

Schopf, P. S., and M. J. Suarez, 1988: Vacillations in a coupled ocean–atmosphere model. *J. Atmos. Sci.,* **45,** 549–566.

Sprintall, J., and M. Tomczak, 1992: Evidence of the barrier layer in the surface layer of the Tropics. *J. Geophys. Res.,* **97,** 7305–7316.

Terray, L., 1998: Sensitivity of climate drift to atmospheric physical parameterizations in a coupled ocean–atmosphere general circulation model. *J. Climate,* **11,** 1633–1658.

Vialard, J., and P. Delecluse, 1998: An OGCM study for the TOGA decade. Part II: Barrier-layer formation and variability. *J. Phys. Oceanogr.,* **28,** 1089–1106.

Webster, P. J., and R. Lukas, 1992: TOGA COARE: The Coupled Ocean–Atmosphere Response Experiment. *Bull. Amer. Meteor. Soc.,* **73,** 1377–1416.

——, V. O. Magaña, T. N. Palmer, J. Shukla, R. A. Thomas, M. Yanai, and T. Yasunari, 1998: Monsoons: Processes, predictability, and the prospects for prediction. *J. Geophys. Res.,* **103,** 14 451–14 510.

Wyrtki, K., 1975: El Niño: The dynamic response of the equatorial Pacific Ocean to atmospheric forcing. *J. Phys. Oceanogr.,* **5,** 572–584.

——, 1985: Water displacements in the Pacific and the genesis of El Niño cycles. *J. Geophys. Res.,* **90,** 7129–7132.

Xue, Y., A. Leetmaa, and M. Ji, 2000: ENSO prediction with Markov models: The impact of sea level. *J. Climate,* **13,** 849–871.

Yu, X., and M. J. McPhaden, 1999: Seasonal variability in the equatorial Pacific. *J. Phys. Oceanogr.,* **29,** 925–947.

Zebiak, S. E., 1989: Oceanic heat content variability and El Niño cycles. *J. Phys. Oceanogr.,* **19,** 475–486.